

Multiferroic monolayers VO*X*(*X*=Cl, Br, I): Tunable ferromagnetism via charge doping and ferroelastic switching

Hong-Chao Yang(杨洪超), Peng-Cheng Liu(刘鹏程), Liu-Yu Mu(穆鎏羽), Ying-De Li(李英德), Kai Han(韩锴), and Xiao-Le Qiu(邱潇乐)

Citation: Chin. Phys. B, 2023, 32 (**6**): 067701. DOI: 10.1088/1674-1056/acaa2b
Journal homepage: http://cpb.iphy.ac.cn; http://iopscience.iop.org/cpb

What follows is a list of articles you may be interested in

Electrostatic switch of magnetic core-shell in 0-3 type LSMO/PZT composite film

Bo Chen(陈波), Zi-Run Li(李滋润), Chuan-Fu Huang(黄传甫), Yong-Mei Zhang(张永梅)
Chin. Phys. B, 2020, 29 (**9**): 097702. DOI: 10.1088/1674-1056/abab73

Structures and local ferroelectric polarization switching properties of orthorhombic $YFeO_3$ thin film prepared by a sol-gel method

Runlan Zhang(张润兰), Shuaishuai Li(李帅帅), Changle Chen(陈长乐), Li-An Han(韩立安), Shanxin Xiong(熊善新)
Chin. Phys. B, 2019, 28 (**3**): 037701. DOI: 10.1088/1674-1056/28/3/037701

Magnetic and ferroelectric properties of Zn and Mn co-doped $BaTiO_3$

Sangram Keshari Das, Binod Kumar Roul
Chin. Phys. B, 2015, 24 (**6**): 067702. DOI: 10.1088/1674-1056/24/6/067702

La-doped $BiFeO_3$：Synthesis and multiferroic property study

Lin Peng-Ting (蔺鹏婷), Li Xiang (李祥), Zhang Li (张丽), Yin Jin-Hua (阴津华), Cheng Xing-Wang (程兴旺), Wang Zhi-Hong (王志宏), Wu Yu-Chuan (吴玉娟), Wu Guang-Heng (吴光恒)
Chin. Phys. B, 2014, 23 (**4**): 047701. DOI: 10.1088/1674-1056/23/4/047701

The magnetoelectric properties of A-or B-site-doped $PbVO_3$ films：A first-principles study

Chen Xing-Yuan (陈星源), Chen Li-Juan (陈丽娟), Zhao Yu-Jun (赵宇军)
Chin. Phys. B, 2013, 22 (**8**): 087703. DOI: 10.1088/1674-1056/22/8/087703

Multiferroic monolayers VOX (X = Cl, Br, I): Tunable ferromagnetism via charge doping and ferroelastic switching

Hong-Chao Yang(杨洪超)†, Peng-Cheng Liu(刘鹏程), Liu-Yu Mu(穆鎏羽), Ying-De Li(李英德), Kai Han(韩锴), and Xiao-Le Qiu(邱潇乐)‡

School of Physics and Electronic Information, Weifang University, Weifang 261061, *China*

(Received 12 October 2022; revised manuscript received 25 November 2022; accepted manuscript online 9 December 2022)

The fascinating properties arising from the interaction between different ferroic states of two-dimensional (2D) materials have inspired tremendous research interest in the past few years. Under the first-principles calculations, we predict the coexistence of antiferromagnetic and ferroelastic states in VOX (X = Cl, Br, I) monolayers. The results illustrate that the VOX monolayers exhibit indirect bandgap characteristics, *i.e.*, their gaps decrease with the halide elements changing from Cl to I. The ground states of all these VOX monolayers are antiferromagnetic (AFM) with the magnetic moments contributed by the V 3d electrons. Furthermore, the magnetic ground state changing from AFM to ferromagnetism (FM) can be realized by doping carriers. In addition, the moderate ferroelastic transition barrier and reversible switching signal ensure their high performances of nonvolatile memory devices. Our findings not only offer an ideal platform for investigating the multiferroic properties, but also provide candidate materials for potential applications in spintronics.

Keywords: antiferromagnetic, ferroelastic, carrier doping, multiferroic states

PACS: 77.55.Nv, 66.30.J– **DOI:** 10.1088/1674-1056/acaa2b

1. Introduction

Recently, two-dimensional (2D) multiferroic materials have attracted significant attention due to the rapid development of nanodevices.[1–5] Typically, more than two ferroic scenarios of FM/AFM, ferroelectricity (FE), and ferroelasticity (FA), are included in multiferroic materials. Such ferroic characteristics can be obtained by polarization-switching, which corresponds to the different orientate directions of magnetic moments, electric dipole moments, and structural distortion, respectively.[6,7] Owing to the coupling effect of the ferroic properties, great opportunities have been brought for applications in spintronics, data storage, and magnetic sensors.[8–13]

The 2D ferromagnetic materials have aroused enormous research interest since the long-range magnetic order in CrI_3 monolayer and $Cr_2Ge_2Te_6$ bilayer have been observed experimentally.[14,15] It is evidenced that 2D ferromagnetic materials possess potential applications in spintronics and miniaturized devices due to the fully polarized current and exotic properties arising from quantum confinement effects.[16–22] As for antiferromagnetic materials, there is neither net magnetic moment nor parasitic stray field, thereby making them robust against perturbation of magnetic fields. The inherent ultrahigh resonance frequency and the unique spin-transport properties of AFM make it different from FM, which leads to promising applications in antiferromagnetic spintronics.[7,23–25] To make better use of magnetic properties, effective approaches have been adopted to achieve the transition from FM to AFM, such as external strain, inducing a heterointerface, and carriers doping.[18,20,26–28] Therefore, tunable 2D magnetic-based multiferroic materials have been investigated extensively. However, FM/AFM-FE multiferroics are rarely reported by virtue of the well-known "d^0 rule".[29,30] Conversely, the FA shows better compatibility with magnetism because that does not require either breaking central-symmetry or partially filled d orbitals.[31,32] It thus holds potential prospects for exploring the FA-based multiferroics at a low dimensional level.[7,33,34] Nevertheless, the scarce researches of the 2D magnetic materials restricted the development of AFM/FM-FA systems.[35–37] Accordingly, by integrating magnetism with ferroelastic characteristics in one material would be ideal for investigating the magnetism-based multiferroics.

In the present work, the coexistence of the AFM and FA in the VOX monolayers is predicted by using the first-principles calculations. The results demonstrate that the VOX monolayers are indirect bandgap semiconductors. The ground states of all these VOX monolayers are AFM with the magnetic moments contributed by the V 3d electrons. By doping carriers, the magnetic ground state changing from AFM to FM can be achieved. Furthermore, the moderate ferroelastic transition barrier and reversible switching signal ensure their high performance of nonvolatile logic and memory devices. These results unveil a desired platform of the VOX single layers, raising the prospects of developing 2D AFM-FA-based multiferroics.

†Corresponding author. E-mail: hc_yang90@163.com
‡Corresponding author. E-mail: qiu.xiaole@163.com

© 2023 Chinese Physical Society and IOP Publishing Ltd

2. Computational methods

The first-principles calculations were carried out by using the density functional theory (DFT) as implemented in the Vienna *ab initio* simulation package (VASP).[38,39] The exchange–correlation interaction was described in the generalized gradient approximation (GGA) within the framework of Perdew, Burke, and Ernzerhof (PBE) functional.[40,41] The electron–ion interaction described by the projector augmented wave (PAW) method was adopted.[42] Considering the possible effect of strongly correlated 3d electrons, we also performed the spin-polar GGA+U calculations throughout the study, and the on-site Coulomb term U for V was chosen to be 1.3 eV according to previous work.[43,44] The cut-off energy was set to 500 eV in the calculations. The convergence criteria for residual force and energy calculation on each atom were set to 0.01 eV/Å and 10^{-5} eV, respectively. A vacuum space of 20 Å was employed to eliminate the interactions between the adjacent periodical structures. The first Brillouin zone was sampled with the Monkhorst–Pack mesh of $11\times11\times1$ and $6\times6\times1$ for the unitcell calculation and supercell calculation, respectively. The ferroelastic transition barrier calculations were carried out by using the climbing-image nudged elastic band (CINEB) method[45] with the force convergence criterion of 0.05 eV/Å. Phonon spectrum calculation was obtained based on the density functional perturbation theory (DFPT) as implemented in the PHONOPY code.[46] A $4\times4\times1$ supercell and a $3\times3\times1$ Monkhorst–Pack k-point mesh were used for the phonon frequencies calculation.

3. Results and discussion

The fully optimized crystal structures of VOX (X = Cl, Br, I) are displayed in Fig. 1. It is a six-layer stacked structure with the stacked sequence of X–V–O–O–V–X along the c direction (see Figs. 1(a) and 1(b)), the corresponding space group is *Pmmn*. Moreover, each V atom is coordinated by four O atoms and two X atoms, which leadsthe octahedral configuration to be distorted strongly. The calculated lattice parameters a and b, the nearest V–V distance d, V–O–V bond angle θ, and magnetic moments μ are listed in Table 1, which accord with previous theoretical and experimental results.[17,43,47] It can be found that the lattice constants increase with the halogen element increasing from Table 1. It is attributed to the fact that the atomic radius turns larger from Cl atom to I atom. The magnetism is contributed by 3d orbits of V atoms, and the net magnetic moment is about 2 μ_B in these VOX monolayers, which is larger than those in their bulk counterparts.[43] To evaluate the bond characteristics of monolayer VOX, the electron localization function (ELF) is exhibited in Fig. 1(d). The strong electronic localization around halide and O atoms indicates that both V–O and V–X are ionic bonds.

Table 1. Calculated values of lattice parameters a and b, the nearest V–V distance d, V–O–V bond angle θ, magnetic moments μ, and bandgap E_g by using GGA+U method at PBE level.

	a (Å)	b (Å)	d (Å)	θ (°)	μ (μ_B/V)	E_g (eV)
VOCl	3.80	3.32	3.15	99.16	1.839	0.88
VOBr	3.82	3.44	3.15	98.66	1.854	0.79
VOI	3.87	3.61	3.15	96.87	1.877	0.42

Table 2. Calculated values of energy of ferromagnetic and four typical antiforromagnetic configurations of VOX (in unit eV).

	VOCl	VOBr	VOI
FM	–162.4	–156.55	–149.55
AFM1	–162.58	–156.66	–149.6
AFM2	–162.27	–156.46	–149.48
AFM3	–162.46	–156.61	–149.58
AFM4	–162.46	–156.56	–149.5

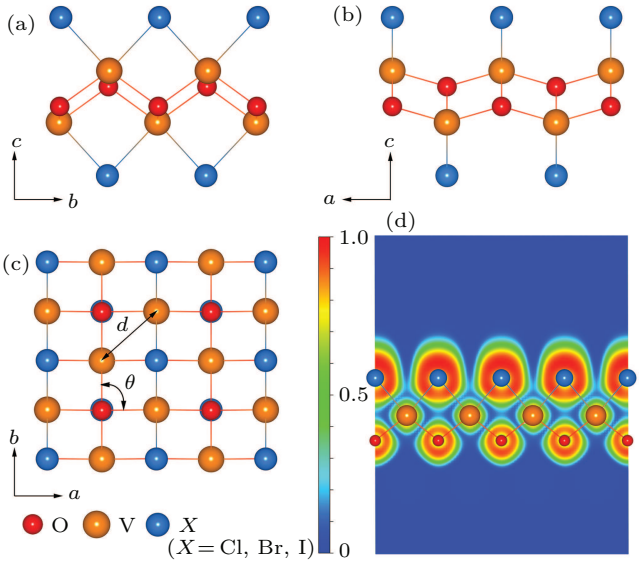


Fig. 1. (a) and (b) Side and (c) top view of the VOX (X = Cl, Br, I) monolayers. Red, orange, and blue balls represent O, V, and halogen atoms, respectively. In panel (c), d and θ represent the nearest V–V distance and V–O–V bond angle, respectively. (d) Electronic localization function (ELF) for VOX monolayers.

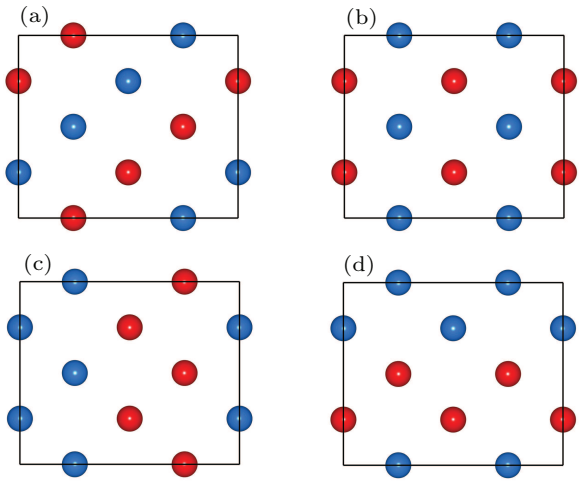


Fig. 2. Four typical antiferromagnetic configurations of VOX monolayers, with blue and red balls representing different spin directions.

To find out the most stable configuration among these materials, we calculate the energy values of ferromagnetic and four typical antiferromagnetic structures of VOX monolayers, which are shown in Table 2 and Fig. 2. It can be obtained that for all these three monolayers, the striped antiferromagnetic state (AFM1) is the magnetic ground state structure, which is in line with the previous research result.[17] It should be emphasized that despite the different stoichiometric ratios of VOX and VOX_2 (X = Cl, Br, I), both of them are stable AFM structures with the same AFM order.[48–50] Consequently, the AFM1 state of each material was selected in the following calculations. According to the ionic valence states, each O atom should gain two electrons and each X atom should gain one electron from the V atom. This trend of charge transfer from V to O and X atoms can be observed in the charge density difference as shown in Fig. 3. From this figure we can see that the electrons around V atoms are depleted, while accumulating near O and X atoms. Therefore, the electrons transfer from V to O and X atoms, leading to the strong ionic bonding, which is consistent with the result of the electron localization function as depicted in Fig. 1(d).

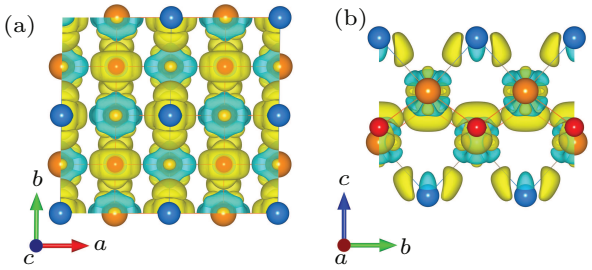


Fig. 3. (a) Top and (b) side view of charge density difference of the monolayer VOCl. The isosurface value is set to 0.01 e/Å^3, with yellow and cyan regions representing electron accumulation and depletion, respectively.

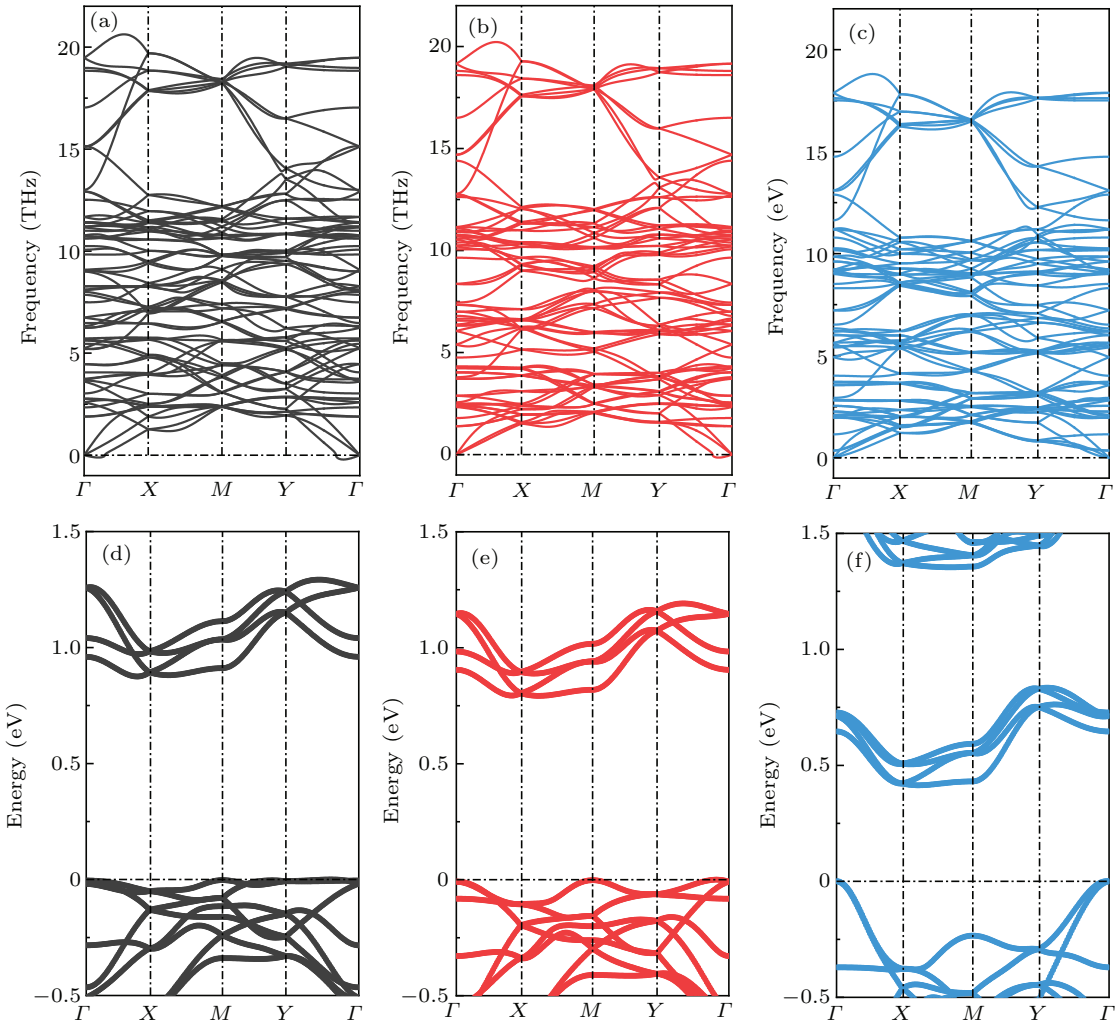


Fig. 4. Phonon spectrum of (a) VOCl, (b) VOBr, and (c) VOI monolayers. Calculated spin-polarized band structures of (d) VOCl, (e) VOBr, and (f) VOI monolayers at the PBE level, with Fermi level set to 0 eV.

The stability of monolayer VOX is investigated by performing the phonon spectrum calculations, and the results are shown in Figs. 4(a)–4(c). No imaginary frequencies are found in the Brillouin zone, which implies that these monolayers are dynamically stable. The band structures of VOX monolayers based on the PBE level are plotted in Figs. 4(d)–4(f). The corresponding values of bandgaps are listed in Table 1, from which we can find that the bandgaps decrease as the halide

element changes from Cl to I. All of these monolayers are semiconductors with indirect bandgap characteristics. Taking monolayer VOCl for example, we further examine the relevant density of states to obtain an in-depth insight into the electronic properties of VO*X* monolayers (see Fig. 5). The results indicate that the CBM of monolayer VOCl is contributed by V-3d$_{xz}$ orbits, while the VBM is predominantly from V-3d$_{xy}$ orbits. The delocalized distribution of projected orbits ensures its strong ionic characteristics, which in accordance with the above discussion.

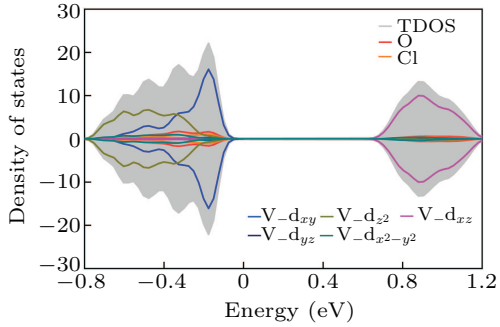


Fig. 5. Total (gray) and atom-projected density of states of monolayer VOCl, with Fermi level set to 0 eV.

Carrier doping is usually considered to be an effective method to improve the magnetic performance of 2D materials.[26,51,52] As shown in Fig. 6(a), we investigated the effect of the magnetic characteristics by doping electrons and holes in VO*X* monolayers. For the electron doping (the negative value of the carrier), it can be found that the exchange energy ΔE increases gradually with the electron concentration increasing for VOCl and VOBr, while VOI exhibits an opposite trend. For the hole doping (the positive value of the carrier), the exchange energy ΔE increases gradually as the doping hole concentration is increased for all these three monolayers. Furthermore, it suggests that increasing the doping carrier concentration can lead the magnetic ground state to convert from AFM into FM for VOCl and VOBr monolayers. As for VOI, it can be found that doping electrons (holes) can enhance its AFM (FM) coupling. Since the competition between the direct-exchange and super-exchange interaction is sensitive to atomic separation and bond angles, it is of great importance to confirm in depth the mechanism of ferromagnetic and antiferromagnetic coupling based on bond angles and bond lengths. Here, taking VOCl for example, we consider V–O–V bond angle θ and V–V bond length d as a function of doped carrier per atom to exhibit a comprehensive understanding of their magnetic properties (see Fig. 6(b)). We can see that with the increase of doping carrier concentration, the direct exchange interaction between the nearest neighboring V–V bond length is gradually elongated, which weakens its AFM of VOCl monolayer. On the contrary, the V–O–V bond angle θ decreases slightly around 90° with carrier concentration increasing, also implying that the super-exchange interaction is FM under high concentration doping according to Goodenough–Kanamori–Anderson (GKA) rules.[53–55] Therefore, the magnetic ground state changing from AFM to FM can be achieved with the carrier concentration increasing, which leads to a great potential application in spintronic devices.

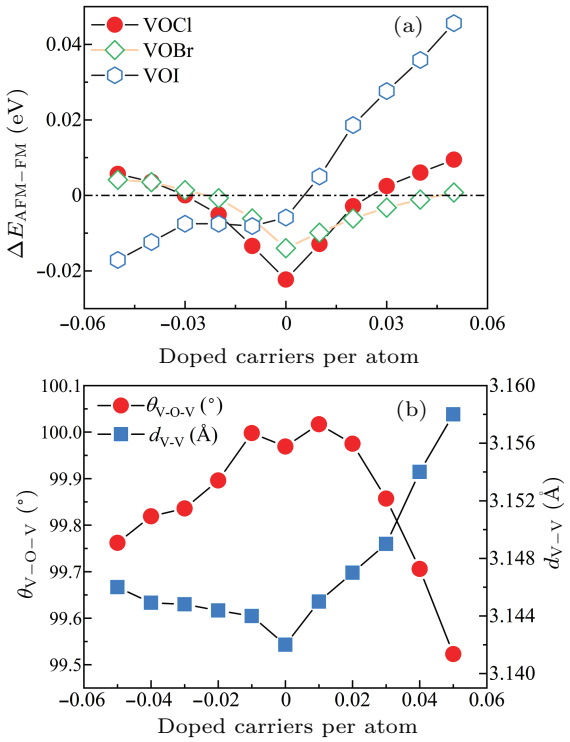


Fig. 6. (a) Curves of exchange energy ΔE *versus* doped carriers per atom for VO*X*. (b) Curves of V–O–V bond angle θ and V–V bond length d *versus* doped carriers per atom for VOCl.

Comparing with VOX_2 monolayers, the higher crystal symmetry and smaller lattice mismatch make VO*X* structure possess potential applications in the area of ferroelastic switching. To this end, the corresponding ferroelastic switching is studied through adopting the climbing image nudged elastic band (CINEB) method, which allows only relaxing atomic distance for each image when keeping the lattice parameters fixed. The initial state (IS) is equivalent to the final state (FS) structure by rotating 90°, the fully optimized lattice constants are shown in Table 1, from which we can find that $a > b$ of the monolayers. Reversible ferroelastic switching between IS and FS can be achieved by applying uniaxial tensile strain along the b axis. And the so-called paraelastic state is a metastable transition state (TS) between the IS and FS, which is simply a square lattice as shown in Fig. 7(a). The corresponding lattice constants of the TS are $a = b = 3.56$ Å, 3.63 Å, and 3.74 Å for VOCl, VOBr, and VOI monolayers, respectively. To probe the metastable property of the TS for these monolayers, the phonon dispersion calculations are adopted in Fig. 8, which shows that all the phonon dispersions exhibit imaginary frequencies in the Brillouin zone, suggesting their instability of the intermediate states.

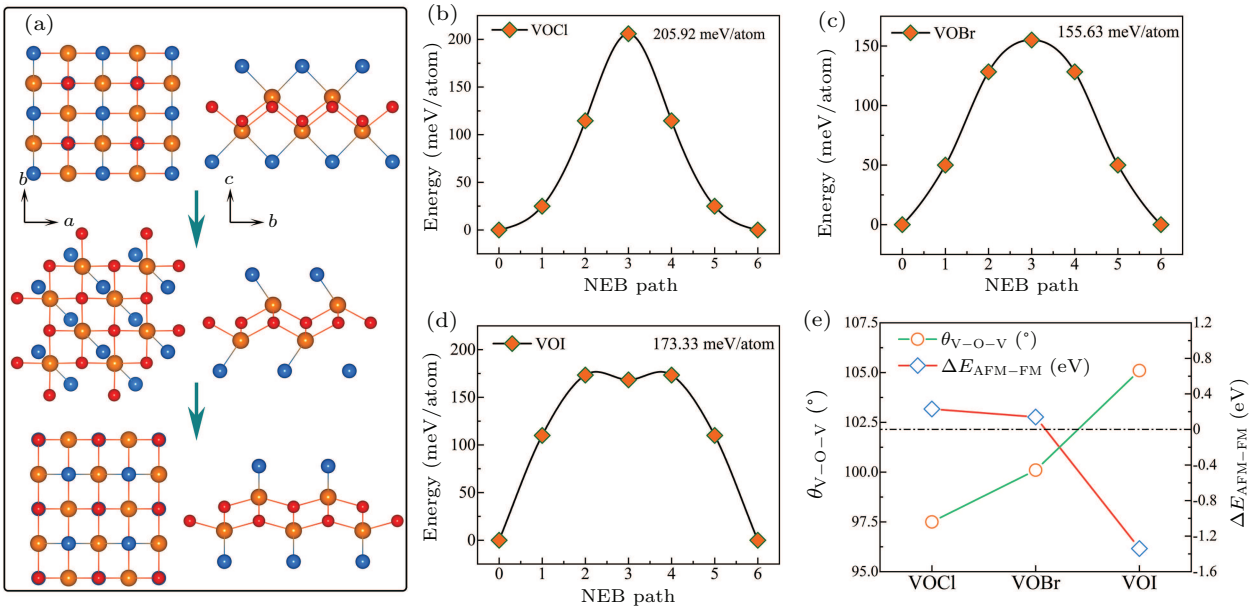


Fig. 7. (a) Left and right columns represent top and side view of initial state (IS), transition state (TS), and final state (FS), respectively. Curves for ferroelastic switching process *versus* step number of (b) VOCl, (c) VOBr, and (d) VOI monolayers. The transition states are obtained by the CINEB method. (e) Calculated V–O–V bond angle and exchange energy ΔE per unit cell of the paraelastic state.

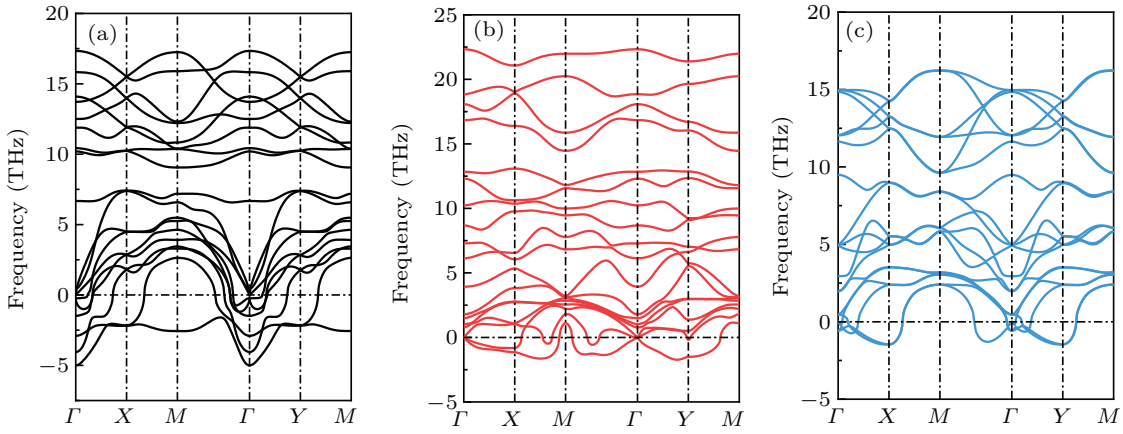


Fig. 8. Calculated phonon spectra of (a) VOCl, (b) VOBr, and (c) VOI monolayers for their paraelastic states.

According to the transformation matrix J obtained by lattice parameters, the transformation barriers calculated based on the Green–Lagrange tensor[56] are 0.21 eV/atom, 0.16 eV/atom, and 0.17 eV/atom for VOCl, VOBr, and VOI monolayers, respectively (see Figs. 7(b)–7(d)). The obtained results are larger than those of phosphorene analogues,[13] InOX (X = Cl, Br) single-layers[57] and t-YN,[58] but smaller than that of BP_5[59] and comparable to those of the candidate ferroelastic 2D materials of CrSX,[60] MnNX (X = F, Cl, Br, I),[61] FeOOH,[7] and GaTeCl.[62] Since the energy barriers of the ferroelastic switching for the above-mentioned systems are in a range of 0.8 meV/atom–320 meV/atom. We thus think that the relatively moderate energy barriers of VOX systems can ensure not only their ferroelastic stability, but also their feasibility in realizing the ferroelastic switching experimentally. Namely, the moderate energy barriers of VOX monolayers demonstrate that the ferroelastic switching can be realized in these materials and resist against the perturbations of external energy. Beside the energy barriers, the reversible switching signal [$\eta = (b/a - 1) \times 100\%$] is another crucial criterion for evaluating ferroelastic performance. According to the lattice constant listed in Table 1, the corresponding switching signals calculated for VOCl, VOBr, and VOI monolayers are 14.5%, 11%, and 7.2%, respectively. Such results unveil that the SL VOX will exhibit a powerful switching signal due to the fact that the typical ferroelastic materials usually have a reversible strain ranging from 0.5% to 3%.[63] For practical applications, the longer and shorter lattices will be reversed frequently in the FA-based nanodevices. Consequently, the relatively small reversible strain of VOX monolayers will lead the ferroelastic switching to be more realizable in experiments than phosphorene (37.9%)[13] and BP_5 (41.4%).[59] Furthermore, we also find that the FM of the paraelastic state is gradually enhanced with the nearest V–O–V angle decreasing, which is consistent with the GKA rule (see Fig. 7(e)). Considering that the ground states of VOCl and VOBr monolayers are AFM, it thus suggests that the FM can be self-regulated by their FA.

4. Conclusions

In summary, our first-principles computations show that VO*X* monolayers are stable multiferroic materials with antiferromagneticity coupling FA. The corresponding magnetic moments are contributed by V 3d electrons. By doping carriers, the magnetic ground state changing from AFM to FM can be realized. Furthermore, the moderate ferroelastic transition barrier and reversible switching signal ensure their high performance of nonvolatile logic and memory devices. In addition, the paraelastic states of VOCl monolayer and VOBr monolayer show the ferromagnetic ground state, suggesting that the FM can be self-regulated by their ferroelastic performance. The multiferroic states of the VO*X* monolayers not only offer a promising platform for studying the multiferroic effects, but also bring the potential application in spintronics.

Acknowledgements

Project supported by the National Natural Science Foundation of China (Grant Nos. 12104344 and 61674003), the Shandong Provincial Natural Science Foundation, China (Grant No. ZR2021QA096), the Science and Technology Development Program of Weifang High-tech Industrial Development Zone, China (Grant No. 2020KJHM03), and the Doctoral Research Start-up Foundation of Weifang University, China (Grant No. 2021BS05).

References

[1] Li L and Wu M H 2017 *ACS Nano* **11** 6382
[2] Tang X and Kou L Z 2019 *J. Phys. Chem. Lett.* **10** 6634
[3] Zhong T T, Li X Y, Wu M H and Liu J M 2020 *Nat. Sci. Rev.* **7** 373
[4] Jia F H, Xu S W, Zhao G D, Liu C and Ren W 2020 *Phys. Rev. B* **101** 144106
[5] You H P, Ding N, Chen J and Dong S 2020 *Phys. Chem. Chem. Phys.* **22** 24109
[6] Hippel A V, Breckenridge R G, Chesley F G and Tisza L 1946 *Ind. Eng. Chem.* **38** 1097
[7] Feng X K, Ma X K, Sun L, Liu J and Zhao M W 2020 *J. Mater. Chem. C* **8** 13982
[8] Spaldin N A and Fiebig M 2005 *Science* **309** 391
[9] Wang P S, Ren W, Bellaiche L and Xiang H J 2015 *Phys. Rev. Lett.* **114** 147204
[10] Taz H, Prasad B, Huang Y L, Chen Z H, Hsu S L, Xu R J, Thakare V, Sakthivel T S, Liu C Z, Hettick M, Mukherjee R, Seal S. Martin L W, Javey A, Duscher G, Ramesh R and Kalyanaraman R 2020 *Sci. Rep.* **10** 3583
[11] Cao L M, Deng X H, Zhou G H, Liang S J, Nguyen C V, Ang L K and Ang Y S 2022 *Phys. Rev. B* **105** 165302
[12] Wang H and Qian X F 2017 *2D Mater.* **4** 015042
[13] Wu M and Zeng X C 2016 *Nano Lett.* **16** 3236
[14] Huang B, Clark G, Navarro-Moratalla E, Klein D R, Cheng R, Seyler K L, Zhong D, Schmidgall E, McGuire M A, Cobden D H, Yao W, Xiao D, Jarillo-Herrero P and Xu X D 2017 *Nature* **546** 270
[15] Gong C, Li L, Li Z L, Ji H W, Stern A, Xia Y, Cao T, Bao W, Wang C Z, Wang Y, Qiu Z Q, Cava R J, Louie S G, Xia J and Zhang X 2017 *Nature* **546** 265
[16] Cheng W R, He J F, Yao T, Sun Z H, Jiang Y, Liu Q H, Jiang S, Hu F C, Xie Z, He B, Yan W S and Wei S Q 2014 *J. Am. Chem. Soc.* **136** 10393
[17] Miao N H, Xu B, Zhu L G, Zhou J and Sun Z M 2018 *J. Am. Chem. Soc.* **140** 2417
[18] Qing X M, Li H, Zhong C G, Zhou P X, Dong Z C and Liu J M 2020 *Phys. Chem. Chem. Phys.* **22** 17255
[19] Guo Y L, Zhang Y H, Yuan S J, Wang B and Wang J L 2018 *Nanoscale* **10** 18036
[20] Sivadas N, Okamoto S, Xu X D, Fennie C J and Xiao D 2018 *Nano Lett.* **18** 7658
[21] Jiang Z, Wang P, Xing J P, Jiang X and Zhao J J 2018 *ACS Appl. Mater. Interfaces* **10** 39032
[22] Yang H C, Song M Q, Li Y D, Guo Y W and Han K 2022 *Physica E* **143** 115341
[23] Baltz V, Manchon A, Tsoi M, Moriyama T, Ono T and Tserkovnyak Y 2018 *Rev. Mod. Phys.* **90** 015005
[24] Jungwirth T, Marti X, Wadley P and Wunderlich J 2016 *Nat. Nanotechnol.* **11** 231
[25] He J J, Ding G Q, Zhong C Y, Li S, Li D F and Zhang G 2019 *Nanoscale* **11** 356
[26] Lv H Y, Lu W J, Luo X, Zhu X B and Sun Y P 2019 *Phys. Rev. B* **99** 134416
[27] Huang B, Clark G, Klein D R, MacNeill D, Navarro-Moratalla E, Seyler K L, Wilson N, McGuire M A, Cobden D H, Xiao D, Yao W, Jarillo-Herrero and Xu X D 2018 *Nat. Nanotechnol.* **13** 544
[28] Shen S Y, Wu Q, Dai Y, Huang B B and Ma Y D 2021 *Phys. Rev. B* **104** 064446
[29] Weston L, Cui X Y, Ringer S P and Stampfl C 2016 *Phys. Rev. B* **93** 165210
[30] Tan H X, Li M L, Liu H T, Liu Z R, Li Y C and Duan W H 2019 *Phys. Rev. B* **99** 195434
[31] Hill N A 2000 *J. Phys. Chem. B* **104** 6694
[32] Spaldin N A, Cheong S W and Ramesh R 2010 *Phys. Today* **6** 38
[33] Kou L Z, Ma Y D, Tang C, Sun Z Q, Du A J and Chen C F 2016 *Nano Lett.* **16** 7910
[34] Tang X and Kou L Z 2019 *J. Phys. Chem. Lett.* **10** 6634
[35] Burch K S, Mandrus D and Park J G 2018 *Nature* **563** 47
[36] Jiang S W, Li L Z, Wang Z F, Mak K F and Shan J 2018 *Nat. Nanotechnol.* **13** 549
[37] Li J H, Li Y, Du S Q, Wang Z, Gu B L, Zhang S C, He K, Duan W H and Xu Y 2019 *Sci. Adv.* **5** eaaw5685
[38] Kresse G and Furthmüller J 1996 *Phys. Rev. B* **54** 11169
[39] Kresse G and Furthmüller J 1996 *Comput. Mater. Sci.* **6** 15
[40] Perdew J P and Wang Y 1992 *Phys. Rev. B* **45** 13244
[41] Perdew J P, Burke K and Ernzerhof M 1996 *Phys. Rev. Lett.* **77** 3865
[42] Blöchl P 1994 *Phys. Rev. B* **50** 17953
[43] Glawion S, Scholz M R, Zhang Y Z, Valentí R, Saha-Dasgupta T, Klemm M, Hemberger J, Horn S, Sing M and Claessen R 2009 *Phys. Rev. B* **80** 155119
[44] Komarek A C, Taetz T, Fernández-Díaz M T, Trots D M, Möller A and Braden M 2009 *Phys. Rev. B* **79** 104425
[45] Henkelman G, Uberuaga B P and Jónsson H 2000 *J. Chem. Phys.* **113** 9901
[46] Gonze X and Lee C 1997 *Phys. Rev. B* **55** 10355
[47] Ekholm M, Schönleber A and Smaalen S V 2019 *J. Phys.: Condens. Matter* **31** 325502
[48] Ai H Q, Song X H, Qi S Y, Li W F and Zhao M W 2019 *Nanoscale* **11** 1103
[49] Song R, Wang B L, Feng K, Wang L and Liang D D 2022 *Acta Phys. Sin.* **71** 037101 (in Chinese)
[50] Zhang Y, Lin L F, Moreo A, Alvarez G and Dagotto E 2021 *Phys. Rev. B* **103** L121114
[51] Abdollahi M and Tagani M B 2020 *J. Mater. Chem. C* **8** 13286
[52] Xiao W Z, Xu L, Xiao G, Wang L L and Dai X Y 2020 *Phys. Chem. Chem. Phys.* **22** 14503
[53] Anderson P W 1950 *Phys. Rev.* **79** 350
[54] Goodenough J B 1955 *Phys. Rev.* **100** 564
[55] Kanamori J 1960 *J Appl. Phys.* **31** S14
[56] Li W B and Li J 2016 *Nat. Commun.* **7** 10843
[57] Xu X L, Ma Y D, Huang B B and Dai Y 2019 *Phys. Chem. Chem. Phys.* **21** 7440
[58] Xu B, Xiang H, Yin J, Xia Y D and Liu Z G 2017 *Nanoscale* **10** 215
[59] Wang H D, Li X X, Sun J Y, Liu Z and Yang J L 2017 *2D Mater.* **4** 045020
[60] Xu B, Li S C, Jiang K, Yin J, Liu Z G, Cheng Y C and Zhong W Y 2020 *Appl. Phys. Lett.* **116** 052403
[61] Hu M L, Xu S W, Liu C, Zhao G D, Yu J H and Ren W 2020 *Nanoscale* **12** 24237
[62] Zhang S H and Liu B G 2018 *Nanoscale* **10** 5990
[63] Wang C S, Ke X X, Wang J J, Liang R R, Luo Z L, Tian Y, Yi D, Zhang Q T, Wang J, Han X F, Tendeloo G V, Chen L Q, Nan C W, Ramesh R and Zhang J X 2016 *Nat. Commun.* **7** 10636